Supporting Information for:

Cyclic constraints on conformational flexibility in γ-peptides: Conformation specific IR and UV spectroscopy

Patrick S. Walsh[†], Ryoji Kusaka[†#], Evan G. Buchanan[†], William H. James III[†a], Brian F. Fisher[‡], Samuel H. Gellman[‡], and Timothy S. Zwier[†]*

†Department of Chemistry, Purdue University, 560 Oval Drive, West Lafayette, IN 47907.

‡Department of Chemistry, University of Wisconsin-Madison, Madison, WI 53706.

#Department of Chemistry, Graduate School of Science, Hiroshima University, Higashi-Hiroshima, 739-8526, Japan.

Table of Contents

1. Comparison of Relaxed Potential Energy Scans along ξ

A comparison of the two calculated relaxed potential energy curves for motion along the ethyl group C-C dihedral is shown in **Figure S1.** The two scans were calculated for the γ_{ACHC} and γ_{ACHC}-H_2O global minimum backbone conformations in the same manner as discussed in the main text. It is immediately clear from the comparison that water only minimally perturbs the shape of the potential energy curves nor the relative energies of the minima. Neither of the potential energy curves have been zero-point corrected. This is a natural consequence of the remote binding of H_2O relative to the ethyl group in the C9(a, g-) conformation of γ_{ACHC}.

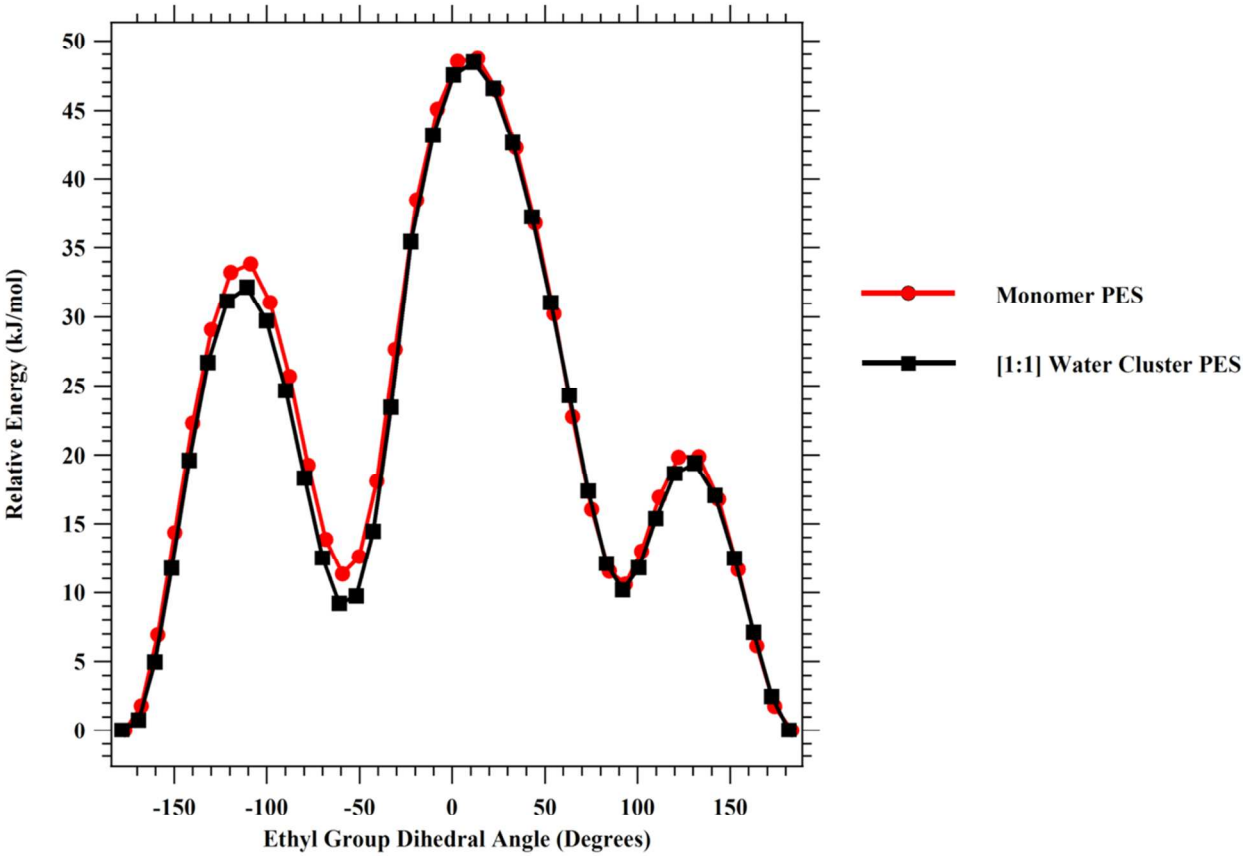

Figure S1. Comparison of the relaxed potential energy curve for internal rotation of the ethyl group in the C9(a,g-) conformer of the monomer and the [1:1] water complex.

2. Comparison of the observed spectrum for γ_{ACHC} with calculated spectra for a wider range of structures

In the main text, the experimental RIDIR spectrum for the observed conformation of γ_{ACHC} was compared with the calculated spectrum for the global minimum, which also provided the best fit with experiment. **Figure S2** shows the calculated scaled harmonic vibrational frequencies and infrared intensities for a selection of other structures that do not match as well. These structural families include a more extended C9(a, a) (6.50 kJ/mol), a C7 (13.19 kJ/mol), an amide stacked conformation (22.11 kJ/mol) and one possessing no hydrogen bonds (8.26 kJ/mol). Structures ii and iv do not match the NH stretch region, while structures I and iii bear a reasonable qualitative resemblance. However, the H-bonded NH stretch of structure (i) is at higher frequency than the global minimum, while the calculated spectrum of the C7 conformer is a reasonable match with experiment, but is much higher in energy.

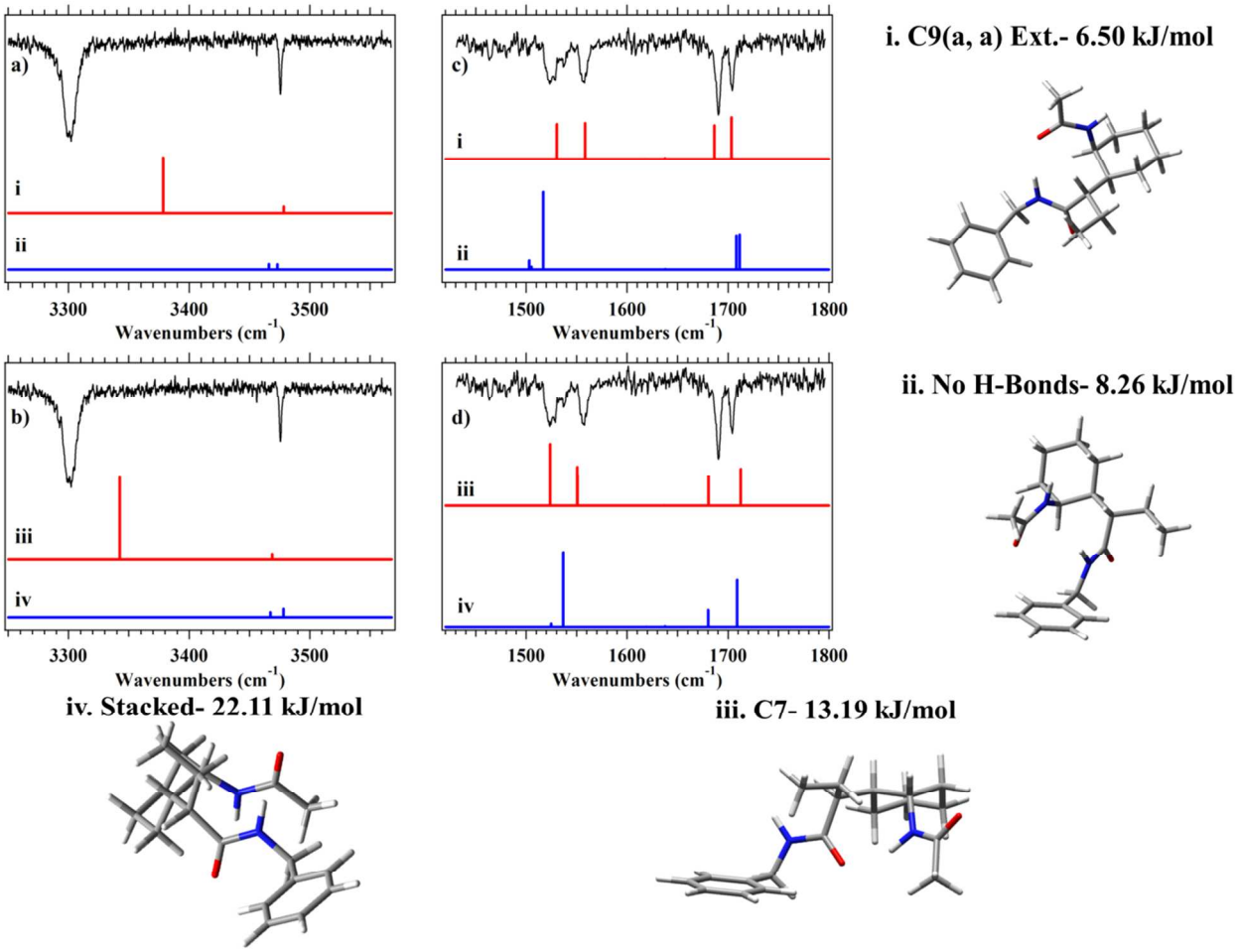

Figure S2. The experimental RIDIR and calculated stick spectra in the NH stretch (a,b) and amide I/II regions (c,d) for γ_{ACHC}. The structures and corresponding spectra are labeled with roman numerals around the outside of the figure (i-iv).

3. Comparison of the observed spectrum for $\gamma\gamma_{ACHC}$ with calculated spectra for a wider range of structures

Conformations belonging to two other low-energy families have been calculated for $\gamma\gamma_{ACHC}$, both of which are double rings. **Figure S3** presents the structures and compares the experimental RIDIR spectra with predicted spectra for the low-lying C9/C9 sequential double ring (7.08 kJ/mol) and the C14/C9 bifurcated double ring (7.82 kJ/mol) conformations. It is immediately clear that these structures reproduce the experimental spectra poorly, and are much higher in energy than the C14 single-ring structure chosen for assignment, which is also the global minimum.

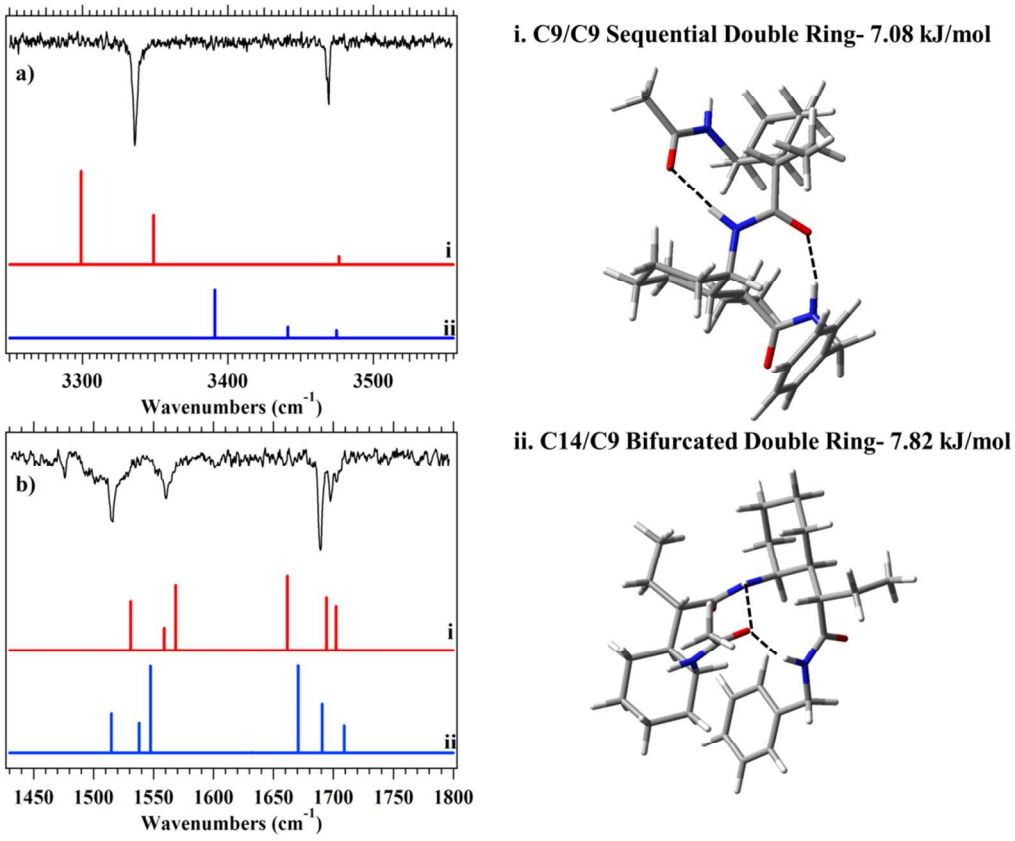

Figure S3. The experimental RIDIR spectra in the NH stretch (a) and amide I/II region (b) along with predicted spectra for two low-energy conformational families of $\gamma\gamma_{ACHC}$. The C9/C9 sequential double ring (i) and C14/C9 bifurcated double ring (ii) families are shown at right of the RIDRIS spectra.

4. Structural Parameters for the Additional Calculated Structures

Relevant structural parameters for the additional low-energy conformations presented in **Figures S2** and **S3** are presented in **Table S1**. These parameters include the backbone dihedral angles, hydrogen bond angles and hydrogen bond distances for the intramolecular H-bonds formed.

	γ_{ACHC} (C9 Ext.)	γ_{ACHC} (No Hydrogen Bonds)	γ_{ACHC} (Stacked)	γ_{ACHC} (C7)	$(\gamma_{ACHC})_2$ (C9/C9)	$(\gamma_{ACHC})_2$ (C14/C9)
Backbone Dihedral	(-104 , 65 , 77 , -106)	(-146 , 57 , 49 , -113)	(-115 , 63 , -72 , 117)	(-161 , 60 , -92 , -121)	(-102 , 65 , 80 , -101)	(-109 , 63 , 78 , -123)
Angles (˚)	(g- , g+ , g+ , g-)	(a , g+ , g+ , g-)	(g- , g+ , g- , g+)	(a , g+ , g- , a)	(g- , g+ , g+ , g-)	(g- , g+ , g+ , a)
(□, θ, ζ, ψ)					(-103 , 64 , 78 , -101)	(-166 , 56 , 53 , -130)
					(g- , g+ , g+ , g-)	(a , g+ , g+ , a)
Sidechain Dihedral	(-178 , 99)	(-179 , 176)	(56 , -96)	(172 , 92)	(-178 , -177 , -79)	(-175 , -50 , -99)
Angles (˚)	(a , g+)	(a , a)	(g+ , g-)	(a , g+)	(a , a , g-)	(a , g- , g-)
(Et_{Nterm},Et_{Cterm},Phenyl)						
rC=O-NH (Å, [Cn_1,Cn_2])	1.97			1.9	(1.97 , 1.89)	(2.11 , 2.41)
C=O←H (˚, [Cn1,Cn2]))	130			109	(131 , 125)	(129 , 120)
O→HN (˚, [Cn1,Cn2]))	156			155	(162 , 169)	(160 , 135)
Interior N-C (Å)			2.99			
Exterior N-C (Å)			2.99			

Table S1. Structural parameters for other representative structures of γ_{ACHC} and $\gamma\gamma_{ACHC}$ optimized using M05-2X/6-31+G(d).

5. Amide Stacked Conformations of Ac-γ^2-hPhe-NHMe-H_2O (γ-H_2O)

In the main text, we focused attention on the family of C9 conformations of γ–H_2O, principally because these structures were analogous to the only structure observed for γ_{ACHC}-H_2O. However, three other conformations of $\boldsymbol{\gamma}$-H_2O were also present in the expansion, in which the H_2O molecule forms as a bridge between the two "layers" of the amide stacked conformation of Ac-γ^2-hPhe-NHMe.[1, 2] Since the two sides of the stack are inequivalent, the water molecule can bind to either side, acting as H-bond acceptor from the NH group and as H-bond donor to the C=O group on the other amide in the stack. In fact, the calculations on γ–H_2O predict that these amide-stacked structures are significantly more stable than the C9 water complexes. We surmise on this basis that the H_2O molecule bridge stabilizes the amide stacked conformation relative to all others, indicating a degree of robustness of amide stacking even in the presence of water due to the H_2O bridges that can be formed. **Figure S4** shows the assigned amide-stacked structures of $\boldsymbol{\gamma}$-H_2O along with the recorded RIDIR spectra for each.[1, 2]

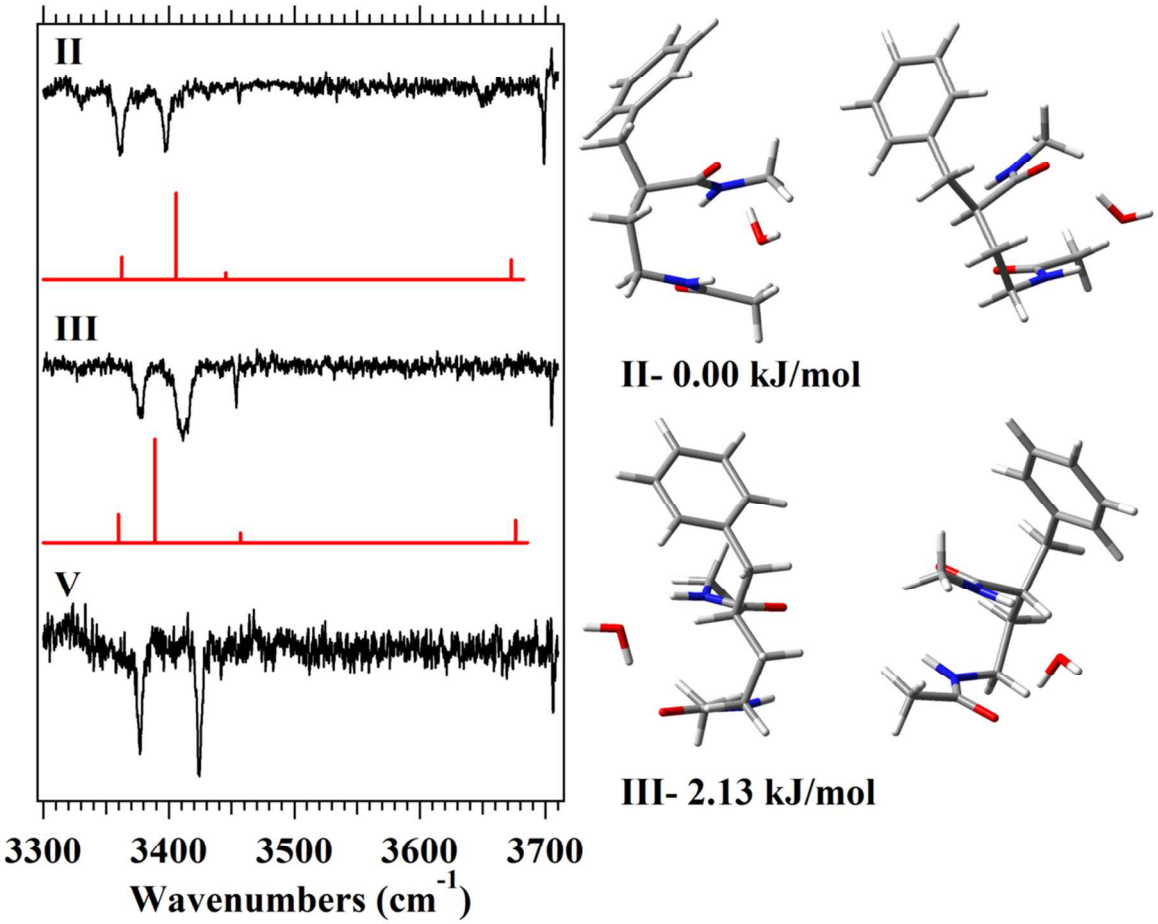

Figure S4. RIDIRS spectra in the NH and OH stretching region of the amide stacked γ-H_2O complexes along with the calculated spectra for the assigned conformations (red). To the right are the structures for the assigned conformations along with their relative energy.

6. Details of the Synthetic Procedures, including NMR Results

O_2N-γ_{ACHC}-γ_{ACHC}-OBn (SI-3):

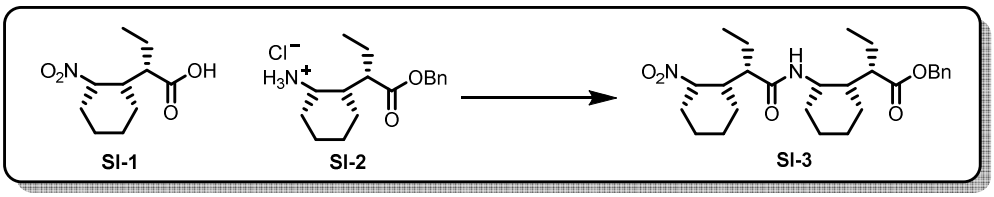

Compounds **SI-1** and **SI-2** were synthesized by previously reported methods.[3] Compound **SI-3** was synthesized by pre-activating a 0.1 M solution of **SI-1** (1.2 eq., 263 mg, 1.22 mmol) in CH_2Cl_2 with EDCI-HCl (235 mg, 1.22 mmol), HOAt (2.04 mL of 0.6 M soln. in DMF, 1.22 mmol), and DIEA (355 µL, 2.04 mmol) for 15 minutes. The pre-activated solution was added to **SI-2** and stirred for 39 hours at room temperature. The reaction mixture was diluted with EtOAc and washed successively with 10% w/w aqueous citric acid, saturated aqueous $NaHCO_3$, and brine. The organic layer was dried with Na_2SO_4, filtered, and concentrated *in vacuo*. The residue was purified *via* silica column chromatography eluting with 5:1 hexanes/ethyl acetate to yield 267 mg pure product as an off-white foam (0.565 mmol, 60% yield). **TLC** R_f = 0.45 (hexanes/EtOAC, v/v, 2:1). **^{1}H NMR** (400 MHz, $CDCl_3$) δ 7.44 – 7.29 (m, 5H), 5.79 (d, *J* = 9.8 Hz, 1H), 5.23 (d, *J* = 12.2 Hz, 1H), 5.00 (d, *J* = 12.2 Hz, 1H), 4.75 (q, *J* = 3.4 Hz, 1H), 4.35 – 4.26 (m, 1H), 2.33 (td, *J* = 10.3, 4.0 Hz, 1H), 2.03 – 0.94 (m, 22H), 0.87 (t, *J* = 7.4 Hz, 3H), 0.86 (t, *J* = 7.4, 3H). **HRMS** *m/z* (ESI): calc. for $C_{27}H_{41}N_2O_5$ $[M+H]^+$ 473.3010, found 473.3016.

O_2N-γ_{ACHC}-γ_{ACHC}-OH (SI-4)

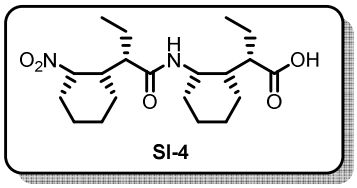

Compound **SI-3** (373 mg, 0.79 mmol) was dissolved in 4 mL MeOH, then charged with 60 mg 10 wt% Pd/C. The reaction vessel was equipped with balloon of H_2 and stirred at room temperature for 7 hours. The reaction mixture was filtered through a bed of Celite and concentrated *in vacuo* to provide 302 mg white solid as pure **SI-4** (quantitative yield). **^{1}H NMR** (300 MHz, $CDCl_3$) δ 6.11 (d, *J* = 9.6 Hz, 1H), 5.13 (bq, *J* = 3.5 Hz, 1H), 4.35 (m, 1H), 2.43 – 1.17 (m, 22H), 0.90 (t, *J* = 7.2 Hz, 3H), 0.86 (t, *J* = 7.2 Hz, 3H). **HRMS** *m/z* (ESI) calc. for $C_{20}H_{35}N_2O_5$ $[M+H]^+$ 383.2541, found 383.2541.

H_2N-γ_{ACHC}-γ_{ACHC}-OH (SI-5)

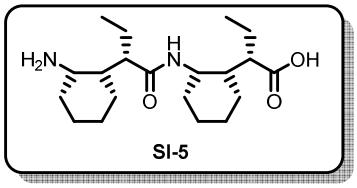

Compound **SI-4** (215 mg, 0.562 mmol) was dissolved in MeOH in a heavy-walled glass pressure vessel. A small scoop (≈0.5g) of Raney Ni in water was washed three times with MeOH and added to the vessel. The vessel was charged with 60 psi H_2 and stirred at room temperature for 36 hours. The vessel was recharged with H_2 after 12 hr, since consumption of H_2 as the reaction proceeded reduced the pressure of H_2 to about 20 psi. The reaction product was filtered through a bed of Celite and concentrated *in vacuo* to yield 183 mg of white solid **SI-5**. This was carried forward without further purification (93% yield). **^{1}H NMR** (400 MHz,CD_3OD) δ 4.06 – 3.97 (bq, 1H), 2.50 (m, 2H), 2.13 – 2.00 (m, 1H), 1.99 – 1.05 (m, 22H), 0.93 (t, *J* = 7.3 Hz, 3H), 0.86 (t, *J* = 7.3 Hz, 3H). **HRMS** *m/z* (ESI) calc. for $C_{20}H_{37}N_2O_3$ $[M+H]^+$ 353.2799, found 353.2800.

Ac-γ_{ACHC}-γ_{ACHC}-OH (SI-6)

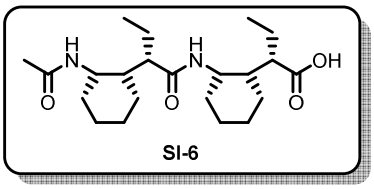

SI-6

Compound **SI-5** (135 mg, 0.382 mmol) and TMSCl (97 μL, 0.764 mmol, 2 eq.) were stirred in 0.2 M dry CH_2Cl_2 at room temperature for 2 hours. The reaction was cooled to 0°C in an ice bath, and DIEA (133 μL, 0.458 mmol, 0.764 mmol, 2 eq.) and Ac_2O (43 μL, 0.458 mmol, 1.2 eq.) were added in succession. The reaction vessel was warmed to room temperature and stirred for 16 hours. After completion, the solvent was removed *in vacuo*, and the crude product was extracted three times with EtOAc from H_2O acidified with 1 M aqueous HCl. The organic fractions were combined, dried with Na_2SO_4, filtered, and concentrated *in vacuo* to produce an orange-brown solid. The residue was purified *via* silica column chromatography eluting with 5% MeOH v/v in CH_2Cl_2 to yield 66 mg white solid **SI-6** (44% yield). **TLC** R_f = 0.22 (5% MeOH v/v in CH_2Cl_2). **^{1}H NMR** (400 MHz, CD_3OD) δ 7.83 (d, *J* = 8.0 Hz, 1H), 4.22 (m, 1H), 4.17 (m, 1H), 2.43 (td, *J* = 10.2, 3.5 Hz, 1H), 2.14 – 2.08 (m, 1H), 2.06 (s, 3H), 1.87 – 1.19 (m, 22H), 0.91 (t, *J* = 7.4 Hz, 3H), 0.82 (t, *J* = 7.3 Hz, 3H). **HRMS** *m/z* (ESI) calc. for $C_{22}H_{39}N_2O_4$ $[M+H]^+$ 395.2905, found 395.2907.

Ac-γ_{ACHC}-γ_{ACHC}-NHBn (SI-7)

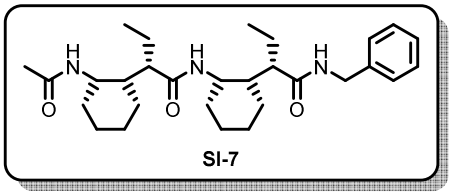

SI-7

Compound **SI-**7 was synthesized by pre-activating a 0.1 M solution of **SI-6** (58.1 mg, 0.147 mmol) in DMF with EDCI-HCl (1.2 eq., 33.9 mg, 0.177 mmol), HOBt (31.8 mg, 0.177 mmol), and DIEA (3 eq., 77 μL, 0.442 mmol) for 15 minutes. The pre-activated solution was added to benzylamine (2 eq., 32 μL, 0.295 mmol), and the solution was stirred for 16 hours at room temperature. The reaction mixture was diluted with EtOAc and washed successively with 10% w/w aqueous citric acid, 5% aqueous LiCl, saturated aqueous $NaHCO_3$, and brine. The organic layer was dried with Na_2SO_4, filtered, and concentrated *in vacuo*. The residue was purified *via* silica column chromatography eluting with 1:2 hexanes/ethyl acetate to yield 51 mg pure **SI-7** as a white foam (0.106 mmol, 72% yield). **TLC** R_f = 0.16 (hexanes/EtOAC, v/v, 1:2).

^{1}H NMR (300 MHz, $CDCl_3$) δ 8.09 (t, *J* = 5.5 Hz, 1H), 7.40 – 7.10 (m, 5H), 6.20 (d, *J* = 8.7 Hz, 1H), 5.78 (d, *J* = 9.0 Hz, 1H), 4.52 (dd, 15.3, 5.8 Hz, 1H), 4.46 (dd, 15.3, 5.8 Hz, 1H) 4.23 (bd, 8.0 Hz, 1H), 3.84 (bd, *J* = 8.9 Hz, 1H), 2.00 (s, 3H), 1.97 – 0.95 (m, 24 H) 0.90 (t, *J* = 7.5 Hz, 3H), 0.85 (t, *J* = 7.5 Hz, 3H). **HRMS** *m/z* calc. for $C_{29}H_{46}N_3O_3$ $[M+H]^+$ 484.3534, found 484.3552.

7. Infrared Ion-Gain (IRIG) Spectrum and Discussion of Results

Infrared ion-gain spectroscopy (IRIGS) is a technique that differs from RIDIR spectroscopy by its choice of UV detection wavelength. While in RIDIR spectroscopy, a UV transition due to a conformational isomer or molecular cluster is chosen in order to selectively detect its IR absorptions, in IRIGS a non-resonant wavelength of the cold molecule just to the red (~180 cm^{-1}) of the S_0-S_1 origin (267.5 nm, ~37383 cm^{-1} in this case) is used. When only conformational isomers of a given molecule contribute to a particular mass channel, IR excitation produces vibrationally excited conformers that possess broad absorptions in the UV that extend to the red of the S_0-S_1 origin, resulting in an ion gain signal at the R2PI probe wavelength built off of zero background. This gain signal is obvious in the IR-UV holeburning scan in **Figure 3b**. When only conformational isomers contribute to the gain signal, the IRIG spectrum produces IR intensities that are a weighted sum of the individual conformational spectra, weighted by their fractional abundances in the expansion.[2, 4]

Figure S5 shows the IRIG spectrum in the γ_{ACHC}^{+} mass channel, obtained with R2PI monitor wavelength of 267.5 nm. We have just proven that the R2PI spectrum in the monomer mass channel contains contributions both from the γ_{ACHC} monomer and from the γ_{ACHC}-H_2O complex. The striking result of this spectrum is that the contributions from the γ_{ACHC}-H_2O complex to the IRIG spectrum are small. The IR transition at 3524 cm^{-1} is the C=O bound OH stretch, the strongest transition in the spectrum of the complex, which is barely visible in the IRIG scan. The RIDIR spectrum of γ_{ACHC}-H_2O (**Figure S5b,** blue trace) scaled to this transition is included beneath the IRIG scan for comparison. In this case, IR excitation of the complex leads to its photofragmentation of the complex by loss of H_2O, producing a γ_{ACHC} monomer with an undetermined amount of internal energy. According to the calculations, the binding energy of

the γ_{ACHC}-H_2O complex is 3053 cm^{-1}, including corrections for zero-point energy and basis set superposition error (BSSE) using the counterpoise method.[5, 6] While it is possible that the choice of monitor wavelength could discriminate against detection of the γ_{ACHC}-H_2O complex if the excess energy in γ_{ACHC} is too small, the most obvious explanation of the reduced intensity in the IRIG spectrum is that the γ_{ACHC}-H_2O complex is present in minor abundance relative to the γ_{ACHC} monomer. Indeed, the IR-UV holeburning scan of **Figure 3c** shows remarkably little gain signal at all UV wavelengths, consistent with a population difference accounting for the relative intensities observed.

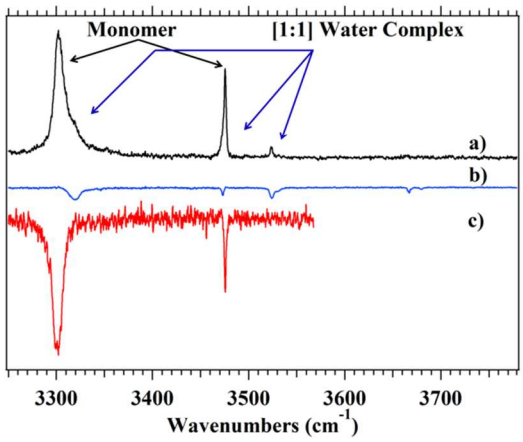

Figure S5. IRIG spectrum (a) taken in the monomer mass channel with the UV fixed at 267.5 nm, just red of the S_0-S_1 origin of the monomer. RIDIR spectra due to the (c) γ_{ACHC} monomer and (b) γ_{ACHC}-H_2O complex, are shown in just below the IRIG spectrum, scaled to match peak intensities. See the text for further discussion.

If true, the present result would add another striking illustration of the fact that the relative intensities in the R2PI spectrum may not accurately reflect relative populations, but instead are dictated by other factors that contribute to the R2PI signal intensity, including Franck-Condon factors, ionization cross sections, or excited state lifetimes. If the IRIG signal is a better

reflection of the relative abundances of monomer and complex in the expansion, one must surmise that the γ_{ACHC}-H_2O complex has an enhanced ionization efficiency in R2PI. By contrast, the amide stacked conformer of Ac-γ^2-hPhe-NHMe showed the opposite trend; namely, its population was greater than its relative intensity in the R2PI spectrum.

REFERENCES

(1) James, W. H., III. Dissertation. Purdue University, West Lafayette, 2009.

(2) Buchanan, E. G.; James, W. H., III; Gutberlet, A.; Dean, J. C.; Guo, L.; Gellman, S. H.; Zwier, T. S. Single-Conformation Spectroscopy and Population Analysis of Model γ-Peptides: New Tests of Amide Stacking. *Faraday Discuss.* **2011,** *150* (0), 209-226.

(3) Guo, L.; Chi, Y.; Almeida, A. M.; Guzei, I. A.; Parker, B. K.; Gellman, S. H. Stereospecific Synthesis of Conformationally Constrained γ-Amino Acids: New Foldamer Building Blocks That Support Helical Secondary Structure. *J. Am. Chem. Soc.* **2009,** *131* (44), 16018-16020.

(4) Dean, J. C.; Buchanan, E. G.; James, W. H.; Gutberlet, A.; Biswas, B.; Ramachandran, P. V.; Zwier, T. S. Conformation-Specific Spectroscopy and Populations of Diastereomers of a Model Monolignol Derivative: Chiral Effects in a Triol Chain. *J. Chem. Phys. A* **2011,** *115* (30), 8464-8478.

(5) Boys, S. F.; Bernardi, F. The Calculation of Small Molecular Interactions by the Differences of Separate Total Energies. Some Procedures with Reduced Errors. *Mol. Phys.* **1970,** *19* (4), 553-566.

(6) van Duijneveldt, F. B.; van Duijneveldt-van de Rijdt, J. G. C. M.; van Lenthe, J. H. State of the Art in Counterpoise Theory. *Chem. Rev.* **1994,** *94* (7), 1873-1885.